VIP MOF Photocatalysis Very Important Paper

International Edition: DOI: 10.1002/anie.201800320
German Edition: DOI: 10.1002/ange.201800320

# Photocatalytic Hydrogen Production Coupled with Selective Benzylamine Oxidation over MOF Composites

*Hang Liu[+], Caiyun Xu[+], Dandan Li, and Hai-Long Jiang**

***Abstract:*** *Photocatalytic water splitting requires separation of the mixed $H_2$ and $O_2$ products and is often hampered by the sluggish $O_2$-producing half reaction. An approach is now reported to address these issues by coupling the $H_2$-producing half reaction with value-added benzylamine oxidation reaction using metal–organic framework (MOF) composites. Upon MOF photoexcitation, the electrons rapidly reduce the protons to generate $H_2$ and the holes promote considerable benzylamine oxidation to N-benzylbenzaldimine with high selectivity. Further experimental characterizations and theoretical calculation reveal that the highly conjugated s-triazine strut in the MOF structure is crucial to the efficient charge separation and excellent photocatalytic activity.*

Photocatalytic hydrogen production by water splitting has been the subject of intense research, as it provides an alternative to replace fossil fuels with clean and renewable energy.[1] Great efforts have been devoted to exploiting highly efficient photocatalysts for this reaction.[2] While the $H_2$-producing half reaction is desired, the other half reaction to produce $O_2$ often suffers from sluggish kinetics and slows down the overall process.[3] To achieve efficient photocatalytic $H_2$ production, most reports on water splitting have focused on this half reaction by consuming holes with diverse sacrificial agents, such as $CH_3OH$, triethanolamine, and triethylamine. On the other hand, as an undesired by-product, $O_2$ is a good electron acceptor that suppresses the $H_2$-producing reduction half reaction and generates system-damaging reactive oxygen species (ROS) by uncontrolled $O_2$ reduction.[4] Moreover, $O_2$ has limited commercial value and is associated with costly separation from $H_2$. In this context, replacing the sacrificial agent consumption or $O_2$ production with organic oxidation would avoid the pollution/waste and enable the synthesis of value-added organic chemicals.[5] Selective oxidative coupling of amines to imines is an important laboratory and commercial procedure because of the versatile applications of imines as biologically active nitrogen-containing organic compounds. This reaction can be promoted with carbocationic species by the activation of photogenerated holes.[6] Therefore, it would be possible to realize simultaneous proton photoreduction and selective amine oxidation in a closed redox cycle over photocatalysts, generating two value-added products, solar fuel and solar chemicals. Unfortunately, related reports remain extremely rare.[5]

In comparison to bulk semiconductors, porous photocatalysts possess unique characteristics with their high surface area, favorable transport of substrates and products, and active-site exposure.[7] In particular, the photogenerated carriers undergo short transport distance to reach the substrates diffused in porous materials, leading to efficient electron–hole (*e-h*) separation and enhanced activity. Metal–organic frameworks (MOFs),[8] a relatively new class of porous crystalline materials featuring highly diversified and tailored structures, have demonstrated their potential for various applications, particularly photocatalysis in recent years.[9–11] The ligands in MOFs absorb light and the photoexcited electrons can be injected into metal–oxo clusters to generate the charge separated state via ligand-to-cluster charge transfer (LCCT), showing semiconductor-like behavior.[9] Quite a few MOFs have been reported for photocatalysis, including water splitting, $CO_2$ reduction, and organic transformations.[9–11] Diverse cocatalysts, especially Pt nanoparticles (NPs), have been shown to greatly enhance the catalytic efficiency.[11]

Herein, a representative MOF, PCN-777 (formulated $Zr_6O_4(OH)_{10}(H_2O)_6(TATB)_2$)[12] with a conjugated 4,4′,4″-(1,3,5-triazine-2,4,6-triyl)tribenzoic acid ($H_3TATB$) ligand, is employed to achieve a complete redox cycle, completing photocatalytic $H_2$ production coupled to selective oxidation of benzylamine to *N*-benzylbenzaldimine, with a Pt cocatalyst in the absence of sacrificial agent (Scheme 1). The photogenerated carriers are effectively separated in PCN-777 with extended π-conjugated ligand, as supported by density functional theory (DFT) calculation and electrochemical measurements as well as control experiments over MOF-808 bearing a similar topology while a short ligand (trimesic acid, $H_3BTC$). Accordingly, PCN-777 has a much higher activity than MOF-808. To our knowledge, this is the first report on coupling $H_2$ production and organic transformation into a redox cycle over MOF photocatalysts.

A novel and rapid microwave-assisted solvothermal approach has been developed, for the first time, to afford PCN-777, which is constructed by $D_{3d}$-symmetric $Zr_6$ antiprismatic units and trigonal-planar organic linkers ($H_3TATB$), featuring a 3D β-cristobalite network (Figure 1 a) with 3.4 nm mesoporous cages (Supporting Information, Figure S1). Powder X-ray diffraction (XRD) profile demonstrates its

[*] H. Liu,[+] C. Xu,[+] Dr. D. Li, Prof. Dr. H.-L. Jiang
Hefei National Laboratory for Physical Sciences at the Microscale, CAS Key Laboratory of Soft Matter Chemistry, Collaborative Innovation Center of Suzhou Nano Science and Technology, Department of Chemistry, University of Science and Technology of China
Hefei, Anhui 230026 (P.R. China)
E-mail: jianglab@ustc.edu.cn
Homepage: http://staff.ustc.edu.cn/~jianglab/

[+] These authors contributed equally to this work.

Supporting information and the ORCID identification number(s) for the author(s) of this article can be found under: https://doi.org/10.1002/anie.201800320.

  

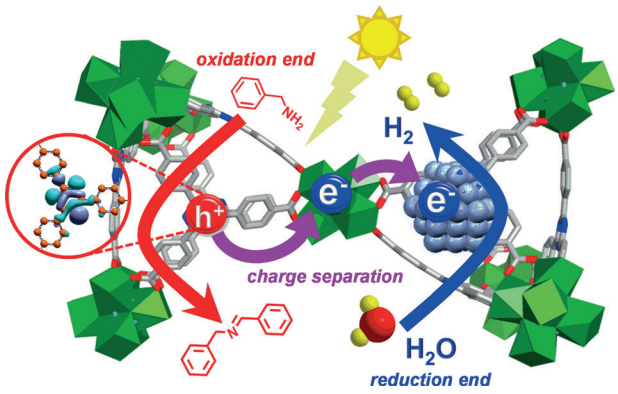


***Scheme 1.*** Illustration of simultaneous proton reduction and selective benzylamine oxidation over Pt/PCN-777 by photocatalysis.

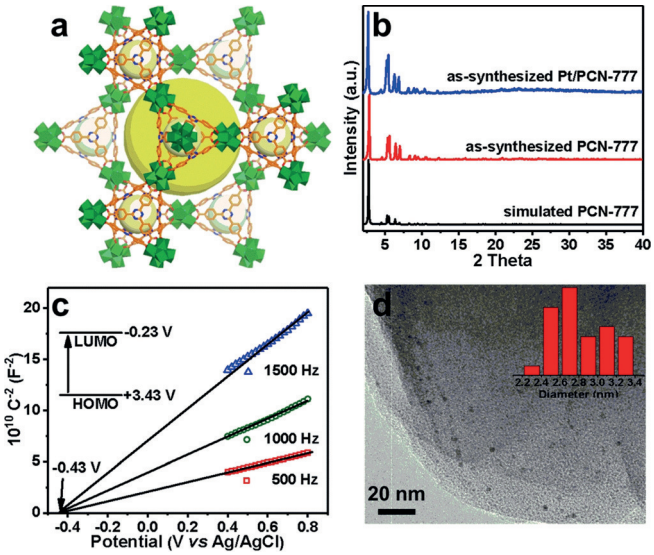


***Figure 1.*** a) View of the 3D structure of PCN-777 along the [111] direction, in which the voids are highlighted by yellow spheres. b) Powder XRD patterns for simulated PCN-777, as-synthesized PCN-777 and Pt/PCN-777. c) Mott–Schottky plots for PCN-777 in a 0.1 M $Na_2SO_4$ aqueous solution (inset: energy-band diagram of PCN-777). d) TEM image for 2.3 wt% Pt/PCN-777 (inset: size distribution of Pt NPs).

high crystallinity and purity (Figure 1b). The high stability ensures its permanent porosity with a high Brunauer–Emmett–Teller (BET) surface area of 1700 $m^2 g^{-1}$ (Supporting Information, Figure S2). Infrared (IR) spectroscopy shows the characteristic absorption at 1521 $cm^{-1}$ for triazine ring (Supporting Information, Figure S3). Mott–Schottky measurements were conducted at the frequencies of 500, 1000, and 1500 Hz (Figure 1c). A positive slope of the $C^{-2}$ values (vs. applied potentials) indicates the character of a typical n-type semiconductor.[10b] The intersection point is independent of the frequency and the flat band position determined from the intersection is −0.43 V vs. Ag/AgCl (that is, −0.23 V vs. NHE), approximate to the bottom of conduction band (LUMO) for n-type semiconductors. With the band gap of PCN-777 estimated to be 3.67 eV according to the Tauc plot (Supporting Information, Figure S4), the top of valence band (HOMO) is then calculated to be 3.43 V vs. NHE. Such an energy-band structure in PCN-777 makes it theoretically feasible for proton photoreduction and photooxidation of organic substrates, such as benzylamine (+0.76 V vs. NHE).[4c]

The Pt/PCN-777 composite, quantified with 2.3 wt% Pt by inductively coupled plasma atomic emission spectrometry (ICP-AES), was fabricated by impregnating PCN-777 in the Pt precursor solution, followed by reduction at 180 °C in a $H_2$/Ar atmosphere. Powder XRD pattern indicates that Pt introduction does not affect the MOF structure and the small sizes of Pt NPs (Figure 1b), which verified by transmission electron microscopy (TEM) observation, showing highly dispersed Pt NPs of about 2.8 nm (Figure 1d).

The photocatalysis has been investigated under different conditions for comparison (Table 1). Pt/PCN-777 exhibits excellent $H_2$ production rate of 586 $\mu mol\, g^{-1} h^{-1}$ in the presence of TEOA as a sacrificial agent (entry 1). The composite is recyclable under the catalytic conditions (Supporting Information, Figure S5). The high activity of Pt/PCN-777 toward $H_2$ production prompts us to replace the sacrificial agent with benzylamine. With the same amount of benzylamine as TEOA, $H_2$ evolution rate decreases to 332 $\mu mol\, g^{-1} h^{-1}$ (entry 2), which can be explained by the weaker electron donating ability of benzylamine than TEOA that slows down the reduction half reaction to some extent. Simultaneously, the benzylamine can be converted to *N*-benzylbenzaldimine at a rate of 486 $\mu mol\, g^{-1} h^{-1}$ with > 99% selectivity (entry 2). Furthermore, Pt/PCN-777 exhibits excellent recyclability and stability in the closed redox cycle involving proton reduction and benzylamine oxidation (Figure 2a; Supporting Information, Figure S6).

***Table 1:*** The activity of photocatalytic $H_2$ production and/or benzylamine oxidative coupling reaction under different conditions.[a]

| Entry | Catalyst | Pt content [wt%] | Benzylamine oxidation rate [$\mu mol\, g^{-1} h^{-1}$] | Sel. [%][b] | $H_2$ rate [$\mu mol\, g^{-1} h^{-1}$] |
|---|---|---|---|---|---|
| 1[c] | PCN-777 | 2.3 | – | – | 586 |
| 2 | PCN-777 | 2.3 | 486 | >99 | 332 |
| 3[d] | PCN-777 | 2.3 | – | – | 73.9 |
| 4[e] | PCN-777 | 2.3 | 1512 | >99 | – |
| 5 | MOF-808 | 2.4 | 128 | >99 | 1.7 |
| 6[f] | MOF-808 | 2.4 | 118.8 | >99 | 1.4 |
| 7[g] | blank | – | 120.6 | >99 | n.d. |

[a] Reaction conditions: 5 mL DMF, 10 mg catalyst, 50 µL benzylamine, 50 µL $H_2O$, 1 atm $N_2$, room temperature, 300 W Xenon lamp. [b] Determined by GC analysis. [c] 50 µL TEOA instead of benzylamine. [d] Without benzylamine/TEOA. [e] Adding 200 mg $AgNO_3$. [f] MOF-808 synthesized by microwave method. [g] For better comparison, the activity was calculated based on 10 mg catalyst.

It is of great importance to elucidate the reaction mechanism behind both half reactions. In the absence of electron donor, the $H_2$ production rate significantly decreases to 73.9 $\mu mol\, g^{-1} h^{-1}$ (entry 3). With $AgNO_3$ as an electron scavenger, benzylamine oxidative coupling reaction proceeds very efficiently at 1512 $\mu mol\, g^{-1} h^{-1}$ in $N_2$ atmosphere (entry 4), suggesting that free electrons and oxygen do not

  

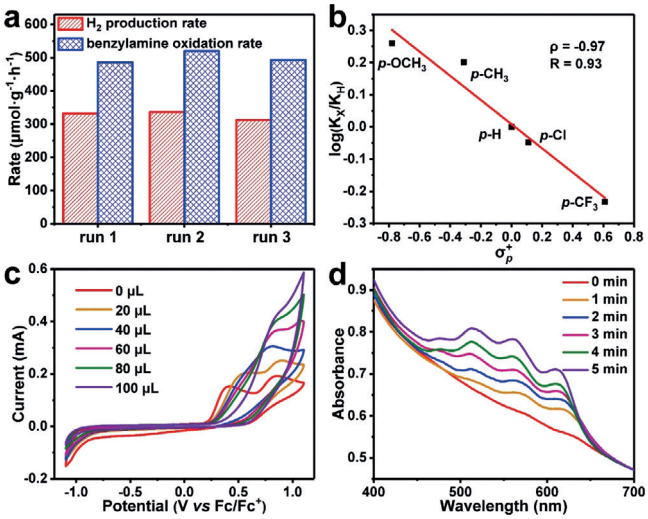


***Figure 2.*** a) Recycling performance of Pt/PCN-777 toward coupling photocatalytic $H_2$ production with selective benzylamine oxidation. b) Hammett plot for the photocatalytic $H_2$ production coupled with selective benzylamine oxidation of *para*-substituted benzylamines over Pt/PCN-777. c) Cyclic voltammetry tests for PCN-777 at different benzylamine concentrations in $CH_3CN$. d) UV/Vis spectra tracking TMPD oxidation along with time in $N_2$ atmosphere over PCN-777 in $CH_3CN$ under light irradiation.

account for the activity while holes on the HOMO play a critical role. The Hammett plot for photocatalytic $H_2$ production coupling with selective benzylamine oxidation of diverse *para*-substituted benzylamines by Pt/PCN-777 has been obtained to identify the key intermediate of benzylamine oxidation (Figure 2b; Supporting Information, Table S2). A reasonable linearity and negative slope infer the generation of carbocationic species ($PhCH_2NH_2^{\bullet+}$) by the holes during the benzylamine oxidation and the resulting carbocationic species couples with benzylamine to give the target product.[4c,6a] The benzylamine oxidative coupling process has been further investigated by cyclic voltammetry measurements (Figure 2c). The first oxidation peak current increases gradually upon the addition of benzylamine, manifesting that benzylamine reacts with holes from the HOMO of PCN-777.[13] Moreover, the significantly enhanced electron paramagnetic resonance (EPR) signal at $g = 2.0027$ can be ascribed to electron-trapped Zr-oxo clusters (Supporting Information, Figure S7), indicating electrons transfer from the TATB ligand during photocatalysis.[10b] Based on the above results, the overall reaction mechanism has been proposed (Supporting Information, Figure S8).

Along with selective benzylamine oxidation, *N*,*N*,*N*′,*N*′-tetramethyl-*p*-phenylenediamine (TMPD) oxidation has been also conducted to examine the oxidative ability of PCN-777. Upon irradiation, the color of TMPD changes from nearly colorless to purple even in a $N_2$ atmosphere. UV/Vis spectra showed that four peaks at 475 nm, 520 nm, 560 nm, and 610 nm belonging to the oxidized products gradually grow along with the irradiation time (Figure 2d),[14] unambiguously demonstrating that the TMPD oxidation promoted by the hole from PCN-777. Taking this one-step further to couple different photooxidation reactions with proton photoreduction, the dibenzylamine oxidative dehydrogenation, and cinnamyl alcohol oxidation have also been attempted. To our delight, the overall redox reactions vividly proceed with the help of electrons and holes under light irradiation (Supporting Information, Table S3). The results indicate general applicability of our approach coupling photocatalytic $H_2$ generation with various organic oxidations over MOF photocatalysts.

To investigate the merits of highly conjugated ligand TATB, trimesic acid ($H_3BTC$) based MOF-808, with the same topology as PCN-777 (Supporting Information, Figure S9), was selected for comparison. After complete characterizations for MOF-808 (Supporting Information, Figures S10–S14), 2.4 wt% Pt/MOF-808 was synthesized with highly dispersed Pt NPs of about 2.30 nm (Supporting Information, Figure S15), via a similar impregnation method to 2.3 wt% Pt/PCN-777. The energy band structure of MOF-808 was quantified based on Tauc and Mott–Schottky plots (Supporting Information, Figures S16, S17). Its LUMO can be determined to be −0.39 V vs. Ag/AgCl (that is, −0.19 V vs. NHE; Supporting Information, Figure S17, inset), similar to that of PCN-777, in accord with the very similar coordination situation of $D_{3d}$-symmetric $Zr_6$ clusters between MOF-808 and PCN-777.

The photocatalytic activity was compared between PCN-777 and MOF-808. The Pt/MOF-808 shows much inferior $H_2$ production rate (ca. 1 $\mu mol\,g^{-1}\,h^{-1}$) (Table 1, entries 5, 6), in comparison to Pt/PCN-777 (Supporting Information, Figure S18). It is worth noting that, in contrast to little activity for $H_2$ production, the oxidation half reaction over Pt/MOF-808 has unmatched activity. The selective benzylamine oxidation proceeds at a relatively low rate even in the absence of catalyst (Table 1, entry 7), which is probably due to the self-coupling between photoexcited benzylamines (Supporting Information, Figure S19).[6b,9c] Furthermore, slight intensity variation of all four peaks related to the TMPD oxidative products over MOF-808 suggest its inferior oxidation ability to PCN-777 (Supporting Information, Figure S20). These results clearly demonstrate that the ligand conjugation in MOFs greatly benefits photocatalysis.

To explain the much higher photocatalytic activity of PCN-777 than MOF-808, we assume that charge separation efficiency would be of paramount importance.[2,11] Photocurrent measurements show that PCN-777 produces a higher photocurrent response than MOF-808, reflecting that photoinduced *e*-*h* pairs are separated more efficiently in the former (Figure 3a). This result is further supported by open circuit

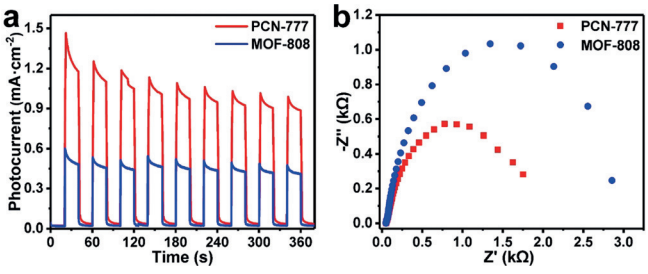


***Figure 3.*** a) Photocurrent tests and b) EIS plots of PCN-777 and MOF-808.

  

photovoltaic measurements, which suggest that photoexcited PCN-777 requires longer time to reach the balance than MOF-808 (Supporting Information, Figure S21). Electrochemical impedance spectroscopy (EIS) for PCN-777 indicates a smaller radius and a lower resistance in charge transportation than those of MOF-808 (Figure 3b). Therefore, PCN-777 possesses higher charge-separation efficiency than MOF-808 with the same topology and the very similar coordination environment of Zr-oxo clusters.

To further explain the difference in charge separation efficiency between PCN-777 and MOF-808, DFT calculation was conducted (Supporting Information, Figure S22).[15] For PCN-777, the HOMO is located mainly at the *s*-triazine unit in the ligand, and the LUMO lies on the Zr-oxo clusters (Supporting Information, Figure S23). The HOMO and LUMO are spatially spaced, so the photogenerated carriers are effectively separated and have relatively long lifetimes. In contrast, both the HOMO and LUMO of MOF-808 are mainly located at the Zr–oxo clusters and the spatial proximity results in a very short lifetime of charge carriers (Supporting Information, Figure S24). The calculation results, together with the above characterization tests, unambiguously suggest that in comparison to MOF-808 featuring the same structural topology, the extended TATB ligand with a highly conjugated system in PCN-777 facilitates its charge separation, thus improving catalytic efficiency.

In summary, we have demonstrated a novel strategy for the integration of photocatalytic $H_2$ production with selective benzylamine oxidation over MOF composites under light irradiation, in the absence of sacrificial agent. The photogenerated electrons reduce protons while the organic transformation to value-added product occurs with the help of holes. The 2.3 wt% Pt/PCN-777 shows much higher activity in the coupled reactions than that of 2.4 wt% Pt/MOF-808, in which both MOFs possess the same structural topology and very similar coordination environment of Zr-oxo clusters. The elongated conjugated ligand in PCN-777 extends the light absorption and greatly improves charge separation, as supported by both experimental and calculation results. To our knowledge, this is the first work employing MOFs as a platform to simultaneously produce a $H_2$ fuel and a valuable organic chemical, and the products are spontaneously separated in the gaseous phase and in the solution, respectively. The coupling strategy developed herein judiciously avoids water oxidation reaction, which is not only of commonly sluggish kinetics but also poses a significant challenge for MOF photocatalysts. We envision that this strategy provides a promising and practical solution to combine solar $H_2$ production with diverse organic oxidation reactions to generate valuable chemicals.

## Acknowledgements

This work is supported by the NSFC (21725101, 21673213, 21521001, 21701160), National Key Basic Research Program of China (2014CB931803), the Recruitment Program of Global Youth Experts, the General Financial Grant from the China Postdoctoral Science Foundation (2016M602018), and the Fundamental Research Funds for the Central Universities (WK2060030029). We thank Prof. Zhiyong U. Wang at Troy University (USA) for fruitful discussions.

## Conflict of interest

The authors declare no conflict of interest.

**Keywords:** amine oxidative coupling · charge separation · hydrogen production · metal–organic frameworks · photocatalysis

**How to cite:** *Angew. Chem. Int. Ed.* **2018**, *57*, 5379–5383
*Angew. Chem.* **2018**, *130*, 5477–5481

[1] N. S. Lewis, D. G. Nocera, *Proc. Natl. Acad. Sci. USA* **2006**, *103*, 15729–15735.
[2] a) Z. Zou, J. Ye, K. Sayama, H. Arakawa, *Nature* **2001**, *414*, 625–627; b) X. Wang, K. Maeda, A. Thomas, K. Takanabe, G. Xin, J. M. Carlsson, K. Domen, M. Antonietti, *Nat. Mater.* **2009**, *8*, 76–80; c) A. Kudo, Y. Miseki, *Chem. Soc. Rev.* **2009**, *38*, 253–278; d) X. Chen, S. Shen, L. Guo, S. S. Mao, *Chem. Rev.* **2010**, *110*, 6503–6570; e) Q. Li, B. Guo, J. Yu, J. Ran, B. Zhang, H. Yan, J. Gong, *J. Am. Chem. Soc.* **2011**, *133*, 10878–10884; f) J. Liu, Y. Liu, N. Liu, Y. Han, X. Zhang, H. Huang, Y. Lifshitz, S.-T. Lee, J. Zhong, Z. Kang, *Science* **2015**, *347*, 970–974; g) Y. An, Y. Liu, P. An, J. Dong, B. Xu, Y. Dai, X. Qin, X. Zhang, M.-H. Whangbo, B. Huang, *Angew. Chem. Int. Ed.* **2017**, *56*, 3036–3040; *Angew. Chem.* **2017**, *129*, 3082–3086.
[3] a) R. D. L. Smith, M. S. Prévot, R. D. Fagan, Z. Zhang, P. A. Sedach, M. K. J. Siu, S. Trudel, C. P. Berlinguette, *Science* **2013**, *340*, 1233638; b) Y. Jiao, Y. Zheng, M. Jaroniec, S. Z. Qiao, *Chem. Soc. Rev.* **2015**, *44*, 2060–2086.
[4] a) J. A. Johnson, J. Luo, X. Zhang, Y.-S. Chen, M. D. Morton, E. Echeverría, F. E. Torres, J. Zhang, *ACS Catal.* **2015**, *5*, 5283–5291; b) D. Sun, L. Ye, Z. Li, *Appl. Catal. B* **2015**, *164*, 428–432; c) Z. J. Wang, S. Ghasimi, K. Landfester, K. A. I. Zhang, *Adv. Mater.* **2015**, *27*, 6265–6270.
[5] a) H. Kasap, C. A. Caputo, B. C. M. Martindale, R. Godin, V. W. Lau, B. V. Lotsch, J. R. Durrant, E. Reisner, *J. Am. Chem. Soc.* **2016**, *138*, 9183–9192; b) G. Han, Y.-H. Jin, R. A. Burgess, N. E. Dickenson, X.-M. Cao, Y. Sun, *J. Am. Chem. Soc.* **2017**, *139*, 15584–15587.
[6] a) F. Su, S. C. Mathew, L. Möhlmann, M. Antonietti, X. Wang, S. Blechert, *Angew. Chem. Int. Ed.* **2011**, *50*, 657–660; *Angew. Chem.* **2011**, *123*, 683–686; b) Q.-Y. Meng, J.-J. Zhong, Q. Liu, X.-W. Gao, H.-H. Zhang, T. Lei, Z.-J. Li, K. Feng, B. Chen, C.-H. Tung, L.-Z. Wu, *J. Am. Chem. Soc.* **2013**, *135*, 19052–19055.
[7] a) Q. Lin, X. Bu, C. Mao, X. Zhao, K. Sasan, P. Feng, *J. Am. Chem. Soc.* **2015**, *137*, 6184–6187; b) W. Zhou, W. Li, J.-Q. Wang, Y. Qu, Y. Yang, Y. Xie, K. Zhang, L. Wang, H. Fu, D. Zhao, *J. Am. Chem. Soc.* **2014**, *136*, 9280–9283; c) V. S. Vyas, F. Haase, L. Stegbauer, G. Savasci, F. Podjaski, C. Ochsenfeld, B. V. Lotsch, *Nat. Commun.* **2015**, *6*, 8508; d) T. Zhang, W. Lin, *Chem. Soc. Rev.* **2014**, *43*, 5982–5993; e) Q. Yang, Q. Xu, H.-L. Jiang, *Chem. Soc. Rev.* **2017**, *46*, 4774–4808.
[8] a) T. R. Cook, Y.-R. Zheng, P. J. Stang, *Chem. Rev.* **2013**, *113*, 734–777; b) H. Furukawa, K. E. Cordova, M. O'Keeffe, O. M. Yaghi, *Science* **2013**, *341*, 1230444; c) H.-C. Zhou, S. Kitagawa, *Chem. Soc. Rev.* **2014**, *43*, 5415–5418; d) T. Islamoglu, S. Goswami, Z. Li, A. J. Howarth, O. K. Farha, J. T. Hupp, *Acc. Chem. Res.* **2017**, *50*, 805–813; e) B. Li, H.-M. Wen, Y. Cui, W. Zhou, G. Qian, B. Chen, *Adv. Mater.* **2016**, *28*, 8819–8860; f) G.

  

Wu, J. Huang, Y. Zang, J. He, G. Xu, *J. Am. Chem. Soc.* **2017**, *139*, 1360 – 1363.

[9] a) M. Alvaro, E. Carbonell, B. Ferrer, F. X. Llabrés i Xamena, H. García, *Chem. Eur. J.* **2007**, *13*, 5106 – 5112; b) Z.-L. Wu, C.-H. Wang, B. Zhao, J. Dong, F. Lu, W.-H. Wang, W.-C. Wang, G.-J. Wu, J.-Z. Cui, P. Cheng, *Angew. Chem. Int. Ed.* **2016**, *55*, 4938 – 4942; *Angew. Chem.* **2016**, *128*, 5022 – 5026; c) C. Xu, H. Liu, D. Li, J.-H. Su, H.-L. Jiang, *Chem. Sci.* **2018**, *9*, 3152 – 3158.

[10] a) Y. Fu, D. Sun, Y. Chen, R. Huang, Z. Ding, X. Fu, Z. Li, *Angew. Chem. Int. Ed.* **2012**, *51*, 3364 – 3367; *Angew. Chem.* **2012**, *124*, 3420 – 3423; b) H.-Q. Xu, J. Hu, D. Wang, Z. Li, Q. Zhang, Y. Luo, S.-H. Yu, H.-L. Jiang, *J. Am. Chem. Soc.* **2015**, *137*, 13440 – 13443; c) H. Zhang, J. Wei, J. Dong, G. Liu, L. Shi, P. An, G. Zhao, J. Kong, X. Wang, X. Meng, J. Zhang, J. Ye, *Angew. Chem. Int. Ed.* **2016**, *55*, 14310 – 14314; *Angew. Chem.* **2016**, *128*, 14522 – 14526; d) A. Dhakshinamoorthy, A. M. Asiri, H. García, *Angew. Chem. Int. Ed.* **2016**, *55*, 5414 – 5445; *Angew. Chem.* **2016**, *128*, 5504 – 5535; e) X.-Y. Dong, M. Zhang, R.-B. Pei, Q. Wang, D.-H. Wei, S.-Q. Zang, Y.-T. Fan, T. C. W. Mak, *Angew. Chem. Int. Ed.* **2016**, *55*, 2073 – 2077; *Angew. Chem.* **2016**, *128*, 2113 – 2117; f) D. Kim, D. R. Whang, S. Y. Park, *J. Am. Chem. Soc.* **2016**, *138*, 8698 – 8701; g) Y. Zhang, J. Guo, L. Shi, Y. Zhu, K. Hou, Y. Zheng, Z. Tang, *Sci. Adv.* **2017**, *3*, e1701162.

[11] a) C. Wang, K. E. deKrafft, W. Lin, *J. Am. Chem. Soc.* **2012**, *134*, 7211 – 7214; b) T. Zhou, Y. Du, A. Borgna, J. Hong, Y. Wang, J. Han, W. Zhang, R. Xu, *Energy Environ. Sci.* **2013**, *6*, 3229 – 3234; c) S. Pullen, H. Fei, A. Orthaber, S. M. Cohen, S. Ott, *J. Am. Chem. Soc.* **2013**, *135*, 16997 – 17003; d) J.-D. Xiao, Q. Shang, Y. Xiong, Q. Zhang, Y. Luo, S.-H. Yu, H.-L. Jiang, *Angew. Chem. Int. Ed.* **2016**, *55*, 9389 – 9393; *Angew. Chem.* **2016**, *128*, 9535 – 9539; e) A. W. Peters, Z. Li, O. K. Farha, J. T. Hupp, *ACS Appl. Mater. Interfaces* **2016**, *8*, 20675 – 20681; f) S. Yang, B. Pattengale, E. L. Kovrigin, J. Huang, *ACS Energy Lett.* **2017**, *2*, 75 – 80; g) X. Fang, Q. Shang, Y. Wang, L. Jiao, T. Yao, Y. Li, Q. Zhang, Y. Luo, H.-L. Jiang, *Adv. Mater.* **2018**, *30*, 1705112.

[12] D. Feng, K. Wang, J. Su, T.-F. Liu, J. Park, Z. Wei, M. Bosch, A. Yakovenko, X. Zou, H.-C. Zhou, *Angew. Chem. Int. Ed.* **2015**, *54*, 149 – 154; *Angew. Chem.* **2015**, *127*, 151 – 156.

[13] a) L.-W. H. Leung, M. J. Weaver, *Langmuir* **1990**, *6*, 323 – 333; b) S. Lin, C. S. Diercks, Y.-B. Zhang, N. Kornienko, E. M. Nichols, Y. Zhao, A. R. Paris, D. Kim, P. Yang, O. M. Yaghi, C. J. Chang, *Science* **2015**, *349*, 1208 – 1213.

[14] Y. Hirata, N. Mataga, *J. Phys. Chem.* **1983**, *87*, 1680 – 1682.

[15] a) C. H. Hendon, D. Tiana, M. Fontecave, C. Sanchez, L. D'arras, C. Sassoye, L. Rozes, C. Mellot-Draznieks, A. Walsh, *J. Am. Chem. Soc.* **2013**, *135*, 10942 – 10945; b) A. S. Yasin, J. Li, N. Wu, T. Musho, *Phys. Chem. Chem. Phys.* **2016**, *18*, 12748 – 12754.

Manuscript received: February 1, 2018
Revised manuscript received: February 27, 2018
Accepted manuscript online: March 6, 2018
Version of record online: March 30, 2018

  